Meteorological aspects of an abnormal cooling event over Iran in April 2009

M. Soltani, C. A. Babu & A. Mofidi

Meteorology and Atmospheric Physics

ISSN 0177-7971

Meteorol Atmos Phys
DOI 10.1007/s00703-014-0309-5

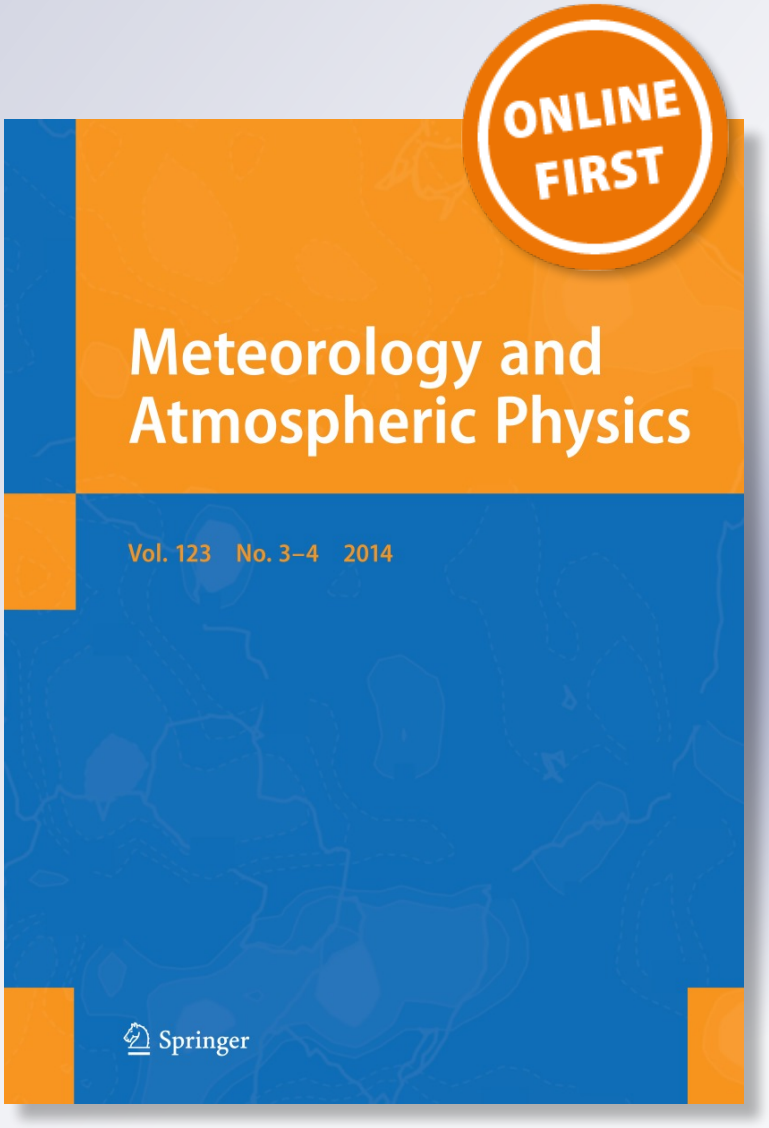

Springer

Meteorol Atmos Phys
DOI 10.1007/s00703-014-0309-5

ORIGINAL PAPER

Meteorological aspects of an abnormal cooling event over Iran in April 2009

M. Soltani · C. A. Babu · A. Mofidi

Received: 18 June 2013 / Accepted: 14 January 2014

Abstract During the period from 12 to 15 April, 2009 nearly the entire Iran, apart from the southern border, experienced an advective cooling event. While winter freezing concerns are typical, the nature of this freezing event was unusual with respect to its date of occurrence and accompanying synoptic meteorological situation. To analyze the freezing event, the relevant meteorological data at multiple levels of the atmosphere were examined from the NCEP/NCAR reanalysis dataset. The results showed that a polar vortex was responsible for the freezing event over the country extending southward extraordinarily in such a way that its ridge influenced most parts of Iran. This was recognized as an abnormal extension of a polar vortex in the recent years. The sea-level pressure fields indicated that a ridge of large-scale anticyclone centered over Black Sea extended southward and prevailed over most parts of Iran. This resulted in the formation of a severe cold air advection from high latitudes (Polar region) over Iran. During the study period, moisture pumping was observed from the Arabian Sea and Persian Gulf. The winds at 1000 hPa level blew with a magnitude of 10 m s^{-1} toward south in the region of convergence (between -2×10^{-6} s^{-1} and -12×10^{-6} s^{-1}). The vertical profiles of temperature and humidity also indicated that the ICE structural icing occurred at multiple levels of the atmosphere, i.e, from 800 hPa through 400 hPa levels. In addition to the carburetor (or induction), icing occurred between 900 and 700 hPa levels in the selected radiosonde stations during the study period. In addition, the HYSPLIT backward trajectory model outputs were in quite good agreement with the observed synoptic features.

Responsible editor: L. Gimeno.

M. Soltani (✉)
Department of Climatology, Faculty of Geography, University of Tehran, Tehran, Iran
e-mail: soltani.clima@gmail.com

C. A. Babu
Department of Atmospheric Sciences, Cochin University of Science and Technology, Cochin 682 016, India

A. Mofidi
Geography Department, Ferdowsi University of Mashhad, Mashhad, Iran

1 Introduction

Frost is the solid deposition of water vapor from saturated air. If a solid surface is chilled below the dew point of the surrounding air and the surface itself is colder than freezing, frost will form on the surface. Frost causes damage to agricultural yield when it destroys plants or hanging fruits and hence affects the economy of the region. Frost is usually identified as one of the most catastrophic natural disasters accompanied by severe losses and damages. Freezing and frost play a significant role in plant phenology of agriculture crops (Alijani and Hajbarpour 2007). Frosts can develop from either thermal (radiative frosts) or dynamical mechanisms (advective frosts).

The radiative frosts occur during the night under calm and cloudless conditions when a temperature inversion is formed near the ground. Frosts are characterized as intense when the intensity of the inversion exceeds 7 °C/20 m and weak when the inversion intensity is less than 3 °C/20 m (Goodal et al. 1957). Radiative frosts are more frequent, causing more serious agricultural hazards and economic impacts, despite their restricted temporal and spatial occurrence. Many plants are damaged or killed by freezing temperatures or frost. This will vary with the type of plant

Published online: 31 January 2014

and tissue exposed to low temperatures. The objective of this paper is to document the salient features of this frost case and to investigate the reasons for their occurrence. This will be accomplished through a combined analysis of routinely available surface and upper level data as well as sounding diagrams. After a brief literature review, frost studies background will be explained in Sect. 1.1, types of frost are demonstrated in Sect. 1.2, cold event description is analyzed in Sect. 2 and data and methodology are illustrated in Sect. 3. The results and discussion are presented in Sect. 4 and finally the major conclusions are summarized in Sect. 5.

1.1 Frost studies background

Several studies on frost and cold waves associated with the synoptic analyses using various techniques over Iran and elsewhere were carried out by researchers. Azizi (2004) carried out an investigation of the synoptic condition leading to vernal extensive frosts in the western half of Iran and found that almost all considerable frosts are followed by a low-pressure system over the northern regions of Iran, while its core located on the center and north of Caspian Sea as well as due to the cold air advections from high latitudes resulting in a cold air influx leading to frost events in the western half of the country. In a similar work, Azizi et al. (2009) attempted to study the unusual cold event of January 2008 by investigating 21 selected stations and comparing the temperature anomaly of January 2008 with the mean long-term minimum temperature of January. They discovered the formation of a blocking system and its effect on the occurrence of intense frosts by looking into the geopotential height and sea-level pressure data. They studied the evolution of atmospheric circulation and associated meteorological parameters involved before and during the frost episode based on synoptic and thermodynamic analysis.

Analysis of the sea-level pressure anomalies during extreme cold temperature days of Iran was carried out by Masoudian (2012). Their results suggest that the least occurrence of extreme colds is for summer, especially in July, which is 0.8 % of the total extreme colds. Roughly speaking, extreme colds are not particular to cold seasons of a year, but it may occur in warm seasons as well. For all patterns, negative temperature anomaly in the southern areas of the country and southern areas of Caspian Sea is trifling due to the atmospheric humidity. Baraty (1999) made an investigation of the synoptic patterns of springtime frosts in Iran. Based on his results, displacement of migrating high-pressure systems from higher latitudes (toward Siberia and central Europe) resulted in extensive and intense frosts. On the contrary, movements from lower latitudes (toward Mediterranean Sea) bring mild and semi-extensive frosts. Frost analysis and prediction in the Kurdistan Province were performed by Soltani et al. (2008) using statistical models. They found that the frequency of freezing days increased in the recent years in Kurdistan.

Omidvar and Ebrahimi (2012) analyzed the cold wave severity between January 6 and 15, 2008 in the central provinces of Iran (Esfahan, Kerman and Yazd provinces). They found that the frost event was those advective cooling events, formed during the study period associated with a strong high-pressure system that was activated over Russia and north of Caspian Sea. Analysis of the synoptic pattern of wintertime frost in Iran was performed by Fattahi and Salehipak (2009). Their results indicate that air types of northern Europe, Siberia and eastern Europe highs played a significant role in the occurrence of intense and extensive frost in the country, respectively. Rahimi (1999) analyzed the frost occurrence probability as well as prediction of the springtime late frosts and autumn early frosts due to their importance for agricultural purposes based on the thermal statistics recorded in the central Alborz Mountain range stations. Investigation of the beginning and end of radiation-advective frosts in northwest Iran was carried out by Nohi and et al. (2007).

In other parts of the world, e.g., South America, analyses were made to investigate the cold events using different techniques. Marengo et al. (1997a), for example, analyzed the climatic impact of cold surges over Amazonia for the 1983–1996 period. Concerning the dynamics of case studies, Marengo et al. (1997b) also studied the polar outbreak that occurred in June 1994, when freezing temperatures affected a large part of the subtropical area of SA, severely damaging coffee and other vegetable-growing areas. The contribution of each individual term within the quasi-geostrophic equation was analyzed, and a feedback-like mechanism between the low- and high-level circulations in the Andes region was proposed during the preliminary phase, which could contribute to intensify the trough further to the east, therefore enhancing the cold advection itself. Garreaud (1999) performed a mesoscale numerical simulation for the 12–15 May 1993 frost episode. Krishnamurti et al. (1999) also studied the precursor conditions for frost over southeastern Brazil. Similarly, Fortune and Kousky (1983) reported on the synoptic evolution of two severe frosts in May 1979 and July 1981 and found some important features preceding freezing temperatures in Brazil, such as a slowly moving long-wave pattern in the central South Pacific Ocean that amplified before the cold event. They also pointed out to the presence of an intense upper-level ridge and trough in southern Chile and eastern Brazil, respectively, which favored the equatorward channeling of cold air.

Vera and Vigliarolo (2000) studied the dynamics of wintertime polar outbreaks, emphasizing the differences

between cases associated with frosts in the subtropical area and cases confined to midlatitudes. In this work, the principal component analysis (PCA) technique was used to extract the most relevant physical patterns. At high levels, some Rossby wave dispersion to the northeast was shown and, at the surface, the wave pattern is normally adjusted following the Rossby topographic waves due to the presence of the Andes. Garreaud (1999) simulated an intermediate event that occurred in May 1993 and proposed the vorticity advection aloft as the main process contributing to the low- and high-pressure intensification at the surface, which is the mechanism associated with low-level cold advection. Furthermore, the subsidence occurring to the south of the subtropical jet also appeared as a relevant mechanism in intensifying the anticyclone, making the jet very important in the process. Finally, Garreaud (2000) complemented the previous studies showing the dynamic structure of wintertime cold waves and suggesting that winter- and summertime cases are very similar, but with different amplitudes. Hamilton and Tarifa (1978) studied the synoptic aspects of a polar outbreak that occurred in the second week of July 1972. The cold air damming event of 6–10 July 1994 was simulated numerically by Bosart et al. (2000).

A comparison of cold events that occurred in Iran and South America, brings out the fact that the cold surges that originated from higher latitudes (Polar region and Siberia high) are mainly responsible for the formation of frosts in Iran, while the large-scale features and topography play a significant role in the majority of frost events in South America.

1.2 Types of frost

Injury to plants from temperature below freezing can be called "frost" or "freezing"; in this study it is referred to as "frost". Plants can also be injured by cold temperature above freezing; this is called "low-temperature injury" or "chilling injury" and is not covered in this paper. There are two types of frost: radiation frost and advective frost (Snyder and Paulo 2005). Radiation frost refers to the white ice crystals, loosely deposited on the ground or exposed objects, which form on cold clear nights when heat losses into the open skies cause objects to become colder than the surrounding air. Soil, buildings, plants and other objects at the Earth's surface act as a heat reservoir by absorbing heat during the day. Plants are damaged when enough heat is lost from this reservoir to lower the temperature at the surface to below critical temperatures. Radiation frost is the most common type of frost in the mountainous regions of Iran.

Advective frost occurs when a mass of cold air displaces a mass of warmer air at the earth's surface. This displacement can be caused by a temperature inversion, which forms when a layer of warm air creates a low ceiling that traps cold air close to the ground. Advective frost can also occur when masses of cold, polar air move into warmer areas. It can occur at any time of day and night. Advective frost is relatively common in the northern half of Iran. Table 1 indicates the characteristics of radiation and advective frosts.

Table 1 Characteristics of a radiation frost and an advective frost (Snyder and Paulo 2005)

Radiation frost	Advective frost
Calm winds—<5 (miles/h)	Winds above 5 (miles/h)
Clear skies	Clouds may exist
Cold air mass 30–200 ft deep	Cold air mass 500–5,000 ft deep
Inversion develops	Protection success limited
Two types: hoar (white) and black	–
Cold air drainage occurs	–
Successful frost protection likely	–

2 Cold event description

A polar vortex affecting Iran resulted in an extensive and intense advective cooling event over most parts of the country during April 12–15, 2009, which was recognized as a peculiar kind of abnormal event since it occurred in April. Figure 1 shows the distribution of the weather stations considered in this analysis throughout the country.

The arrival, development and leaving of the advective frost during a 4-day timescale from 12 April to 15 April 2009 over Iran are illustrated in Fig. 2. Therefore, the minimum temperature values were interpolated to indicate the shifting of the cold system during the study period over the area. Isotherm maps indicate that most stations affected severely by the arrival of the cold system into the country from the northwest showed a drastic decrease in temperature and occurrence of snowfall in some parts of the mountainous areas on April 12, 2009 (Fig. 2a). On the next day, the cold system was more intense (Fig. 2b). No remarkable variation in the intensity of the cold system was noticed on April 14, 2009. However, most stations experienced an intense cooling and a substantial fall in temperature due to the cold air advection associated with the system and the most intense drop in temperature took place on this day.

Pollution station (35°43′N, 52°24′E) in the Tehran Province, for instance, located over the Alborz Mountain range recorded the lowest temperature (−12 °C). Furthermore, Chalderan (39°04′N, 44°23′E) in Western Azerbaijan Province (northwest of Iran) and Bostanabad (37°51′N, 46°51′E) in Eastern Azerbaijan Province (northwest of Iran) weather stations with −11 and −10 °C, respectively,

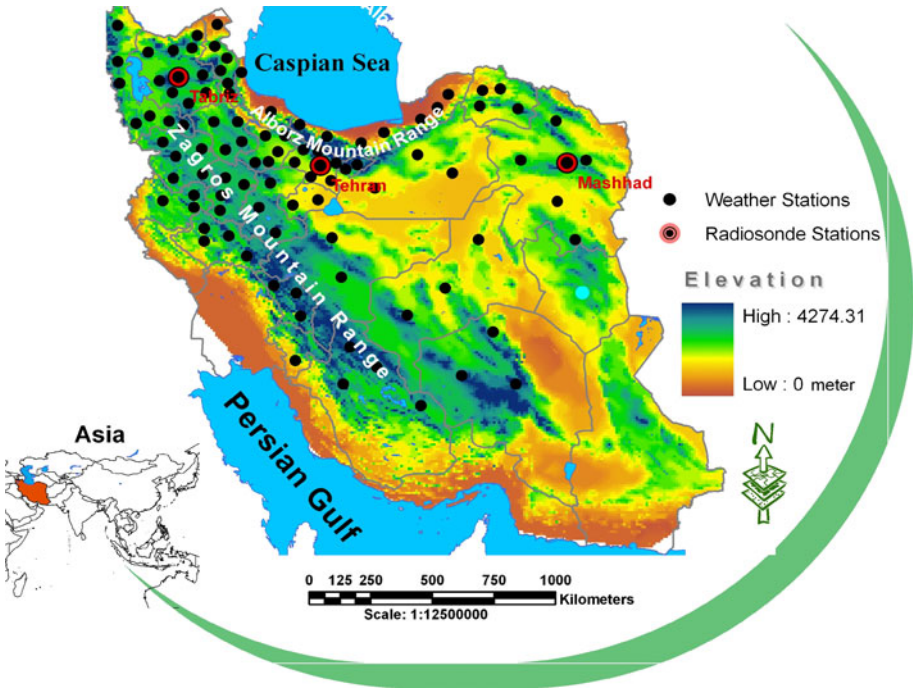

Fig. 1 Geographic position of Iran and distribution of 100 weather stations and 3 radiosonde stations considered in the study and the underlying topography

recorded the next extreme values (Fig. 2c). The last day of the cold system activity happened in the northeastern parts of the country on April 15, 2009 resulting in a decrease in temperature over the regions. On the contrary, the minimum temperature over the west and northwest areas started to rise gradually on April 15, 2009 in comparison with the previous days (Fig. 2d). Figure 2 also indicates that the weather stations located mostly in the mountainous regions, such as Alborz and Zagros Mountain range, recorded the lowest temperature as well as the severest frost compared to those of the non-mountainous territories, as the extreme minimum temperature events happened in the high altitudes.

A primary investigation of the cooling event, which described its activity over the country in Fig. 1, indicates that it was caused by the extra-extension of the polar vortex toward the lower latitudes in such a way that countries such as Iran were affected largely by its trough, resulting in an extensive advective cooling event across the country due to the cold air advection (Fig. 3). Accordingly, the mean surface air temperature anomaly (shaded) in April 2009 and mean surface temperature (pink contours) in April during the period of 1950–2009 clearly shows that a severe cold event in April 2009 occurred as compared to the mean temperature values for a 60-year period (Fig. 3).

In addition, the box and whisker plots of time series, which clearly show the shape of the distribution, central values and variability of the minimum and maximum temperature, sea-level pressure and total cloud cover values, illustrate that the minimum and maximum temperature values have a positive and ascending trend from the beginning toward the end of April. This is a common trend, although, from April onward, the air begins to rise toward the summer (based on Iranian calendar, 22 March is recognized as the 1st day of the spring season and the *New Year* in Iran). But there is a gap in the series during the study period, which is marked with a red closed circle. Both minimum and maximum temperature values decreased dramatically even more than in the past records in April (Fig. 4a, b). The condition for sea-level pressure and total cloud cover is opposite. The meaning is that they increased during the same period (Fig. 4b, d).

The climate of Iran, on the whole, varies from north to south. On the northern edge of the country (the Caspian coastal plain) temperatures rarely fall below freezing and the area remains humid for the rest of the year. Summer temperatures rarely exceed 29 °C (84.2 °F). To the west, settlements in the Zagros basin experience lower temperatures, severe winters with below 0 °C average daily temperatures and heavy snowfall. In the eastern and central parts of the country, the average summer temperatures exceed 38 °C (100.4 °F). In general, January is the coldest month, with temperatures from 0 °C to 10 °C, and August is the hottest month from 20 °C to 30 °C or more for most regions in Iran (Alijani 1996). The winter months in Iran begins from 22 December and continues to 21 March. The long-term (35-years) interpolation of annual and April minimum and maximum temperature values for Iran are presented in Fig. 5. According to the figure, annual minimum temperatures mostly occur in the west and northwest of the country (Fig. 5a), while the opposite is true for the

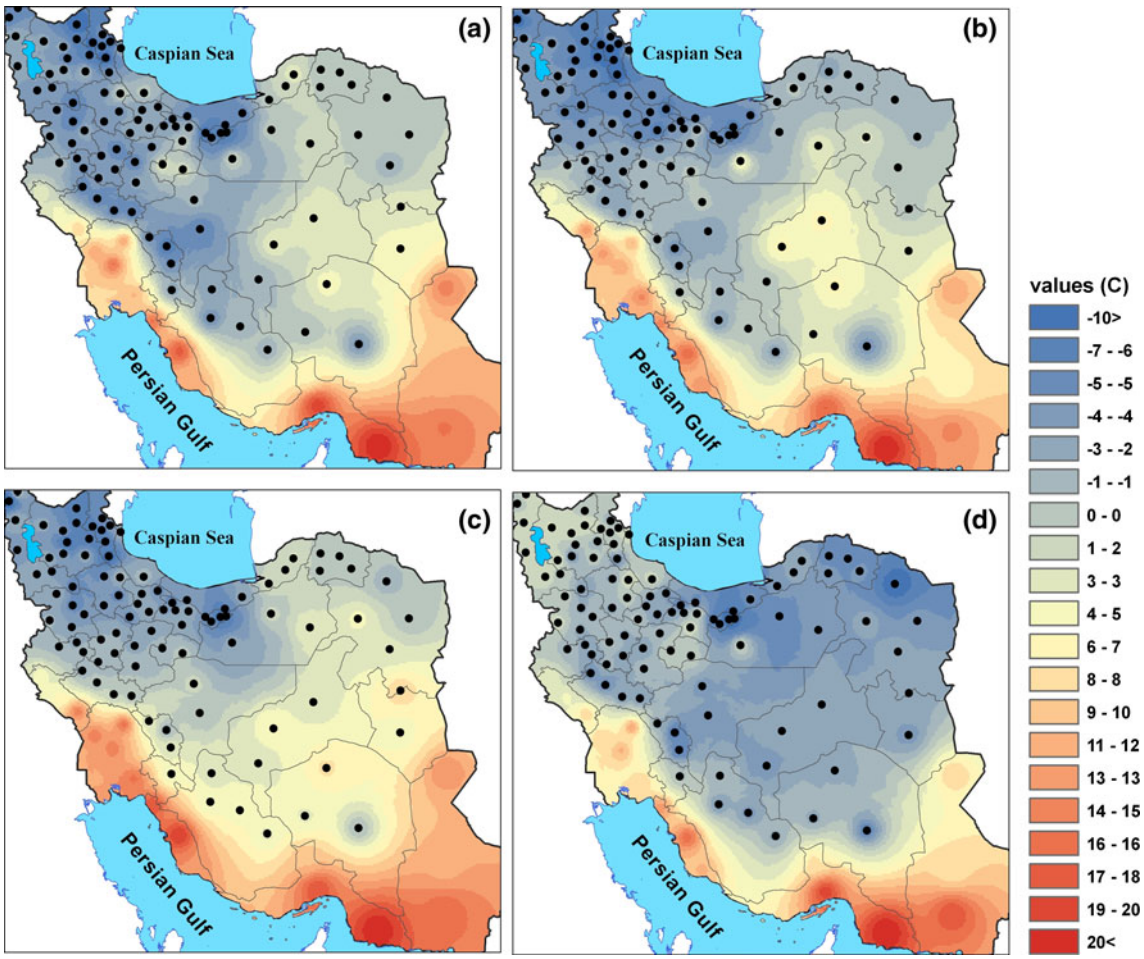

Fig. 2 The minimum temperature (°C) values interpolation valid on **a** April 12, **b** April 13, **c** April 14, **d** April 15, 2009. The isotherm charts were produced using Arc GIS. It may be noted that the minimum temperatures for more than 100 stations were used for interpolation (a few stations were added for the southern border of Iran) to avoid error in interpolation

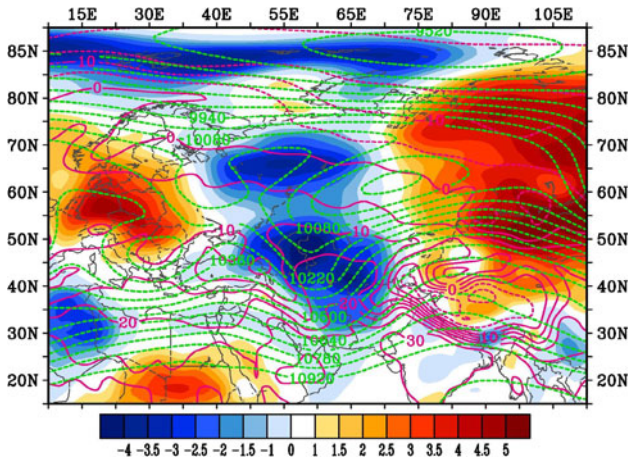

Fig. 3 Chart of average temperature during the period of 1950–2009 in °C (*pink contours*) and anomaly temperature in °C (*shaded*) in April 2009; and 250 hPa geopotential height in m (*dashed green contours*) on April 13, 2009

maximum temperatures, which mainly happen in the central and southeastern parts of the country (Fig. 5c). Surprisingly, we found that the minimum and maximum temperature values in April months are similar not only in terms of values, but also have a quite similar spatial distribution compared to the annual pattern (Fig. 5b, d). It means that April in Iran is not usually considered as a very cold month for severe frost events to take place compared to, e.g., December, January and February months.

Additionally, to illustrate that this cooling event, which occurred in April 2009, was kind of abnormal and unusual in terms of the date of occurrence as well as to present the fact that April 2009 has been the coldest month for at least the past 35 years, we produced time series of the maximum and minimum temperature values for both annual and April in Tabriz, Mehrabad (Tehran) and Esfahan stations, each one representing a different geographical location of the country, i.e., northwest, north and central regions,

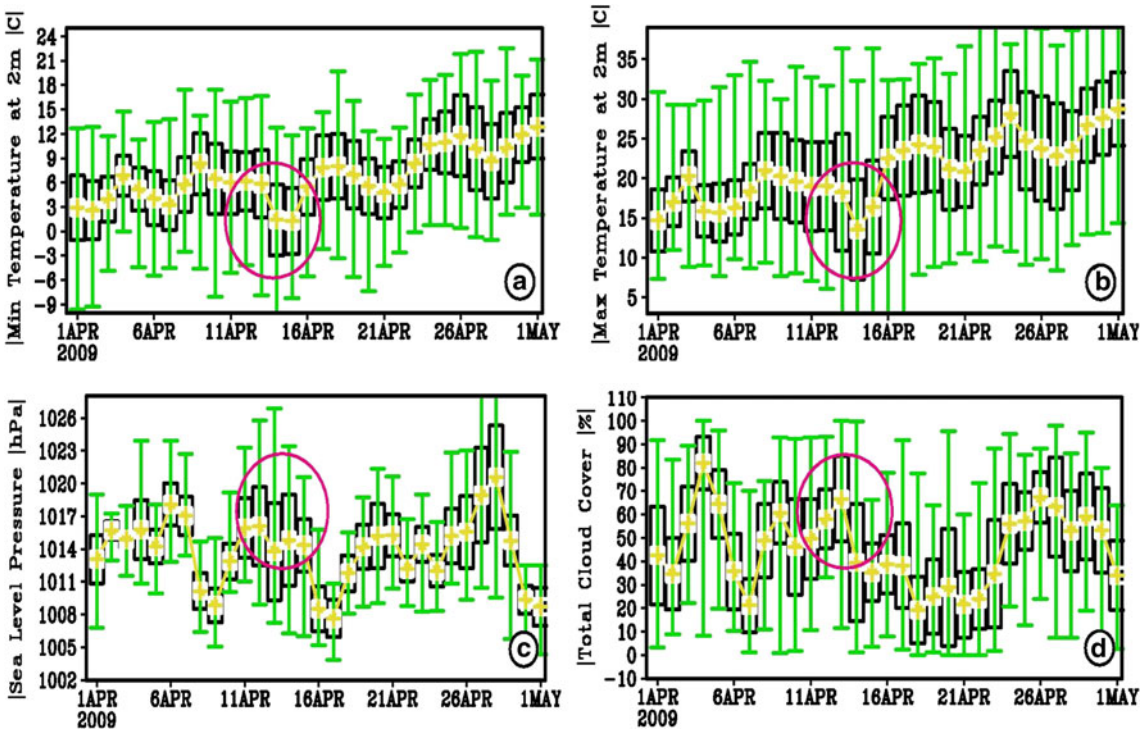

Fig. 4 Box and whisker plots time series: **a** median (*yellow line*), lower and upper quartiles (*black boxes*), and lower and upper extreme values (*green bars*) calculated to draw daily minimum temperature (°C) over the area north of 30°N, south of 40°N, east of 45°E and west of 65°E, from 1 April to 31 April 2009. **b–d** are same as **a**, but for maximum temperature, sea-level pressure and total cloud cover, respectively

respectively. It may be noted that the time series values for southern Iran was excluded, because based on the climatology records no significant cooling events have been recorded for that region. It can be seen that, based on Fig. 6, the minimum temperature values in April 2009 for the selected stations dropped dramatically to the lowest values for the entire period, which is marked with a green circle on the plots, while the decrease in maximum values is not significant for the same period. In terms of values in April 2009, the lowest minimum temperature occurred in Tabriz station with 4.5 °C (Fig. 6a), while the highest maximum temperature took place in Esfahan with 26 °C (Fig. 6f); this is common due to the topography and geographical location of the stations. All these factors discussed above indicate that an unusual and abnormal cooling event occurred over Iran. It is therefore necessary to analyze and understand such a severe phenomenon, as frost occurred nationwide as reported in all the weather stations except in the southern coasts of Iran.

3 Data and methodology

To study the synoptic features and the reasons for the severe advective cooling event during 12–15 April 2009, the following meteorological elements or derived parameters are employed: relative vorticity (10^{-5} s^{-1}), geopotential height (m), 500 hPa pressure fields, minimum, maximum and mean air temperatures (°C), *sea-level pressure* (SLP), 1,000–500 hPa thickness, u and v wind components (m s^{-1}), relative humidity (%), divergence, convergence of wind fields (10^{-6} s^{-1}), total cloud cover (%) and temperature advections (K/day). Therefore, the required data sets were obtained from NCEP/NCAR reanalysis product (Kalnay 1996), derived parameters were analyzed and the meteorological charts were prepared (Dotty 1996). The thermodynamic structure of the atmosphere during the frost event was studied employing the skew-t sounding diagrams as well. The upper air data sets were selected from the Wyoming University website for selected weather stations and then the vertical profiles generated by using *RAwinsonde OBservation program* (RAOB).

Meteorological satellite images for the study period were selected from the Dundee satellite receiving station (2012), UK. In addition, the HYSPLIT (Hybrid-Single Particle Lagrangian Integrated Trajectory) model, developed by NOAA ARL, was used to compute the backward trajectories discussed in this study (Draxler and Rolph 2011; Rolph 2011). Each backward trajectory was calculated for 48 h duration with three ending levels [500, 1,500

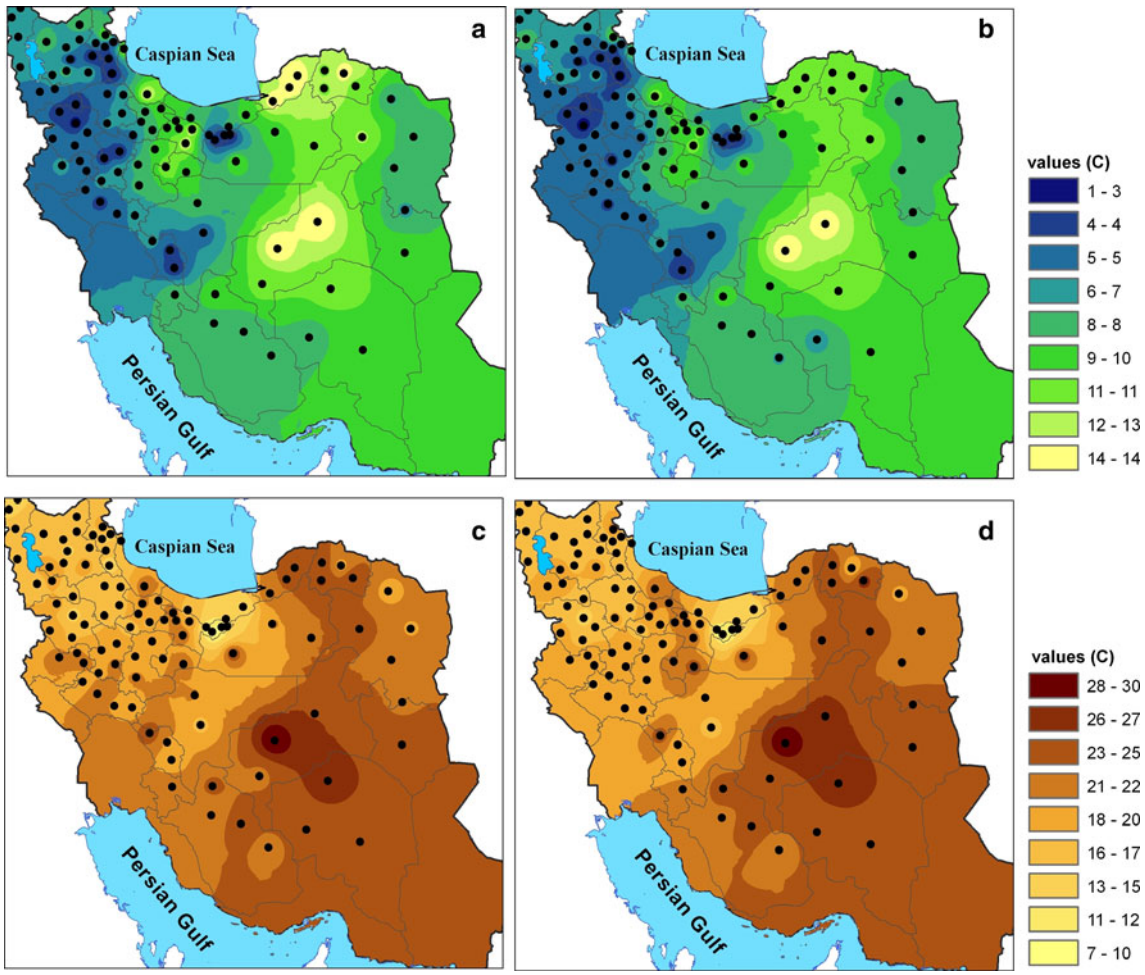

Fig. 5 Minimum and maximum temperature (°C) value interpolation: annual values (**a**, **c**) and April values (**b**, **d**), respectively, for a 35-year period, i.e, from 1976 to 2010 for Iran

and 5,000 m above ground level (AGL)]. The meteorological input for the trajectory model was the reanalysis dataset. HYSPLIT uses archived three-dimensional meteorological fields generated from observations and short-term forecasts (Stunder 1997). Radiosonde profiles from three stations in Iran were considered for the analysis during April 12 to 15, 2009 as shown in Fig. 1. It is not surprising to note that approximately 70 % of the weather stations experienced frost for at least 1 day, being situated in mountainous areas (Alborz and Zagros Mountain range).

4 The results and discussion

4.1 Weather maps and sounding diagrams analyses

In this section, the meteorological elements such as u and v wind components, mean pressure, relative humidity and temperature fields at multiple levels of the atmosphere along with the skew-t thermodynamic diagrams during a period of April 12 to 14, 2009 were investigated. During the study period, most parts of Iran were affected by cold air advection from high latitudes (Polar region) and this resulted in an intense and extensive late advective cooling event in the country.

4.1.1 Weather chart analysis on April 12, 2009

The 500 hPa level relative vorticity and geopotential height on April 12, 2009 are shown in Fig. 7a. As the contours indicate, the polar vortex largely extended southward and its ridge influenced most parts of the low latitude regions of Iran. This was relatively an unusual extension of the polar vortex. As a result, a closed low center with central geopotential height of 5,400 gpm on longitude 60°E and latitude 55°N, extended over Iran. On this day, i.e., April 12, 2009, the positive relative vorticity was evident, coinciding with the low center (in the geopotential height field)

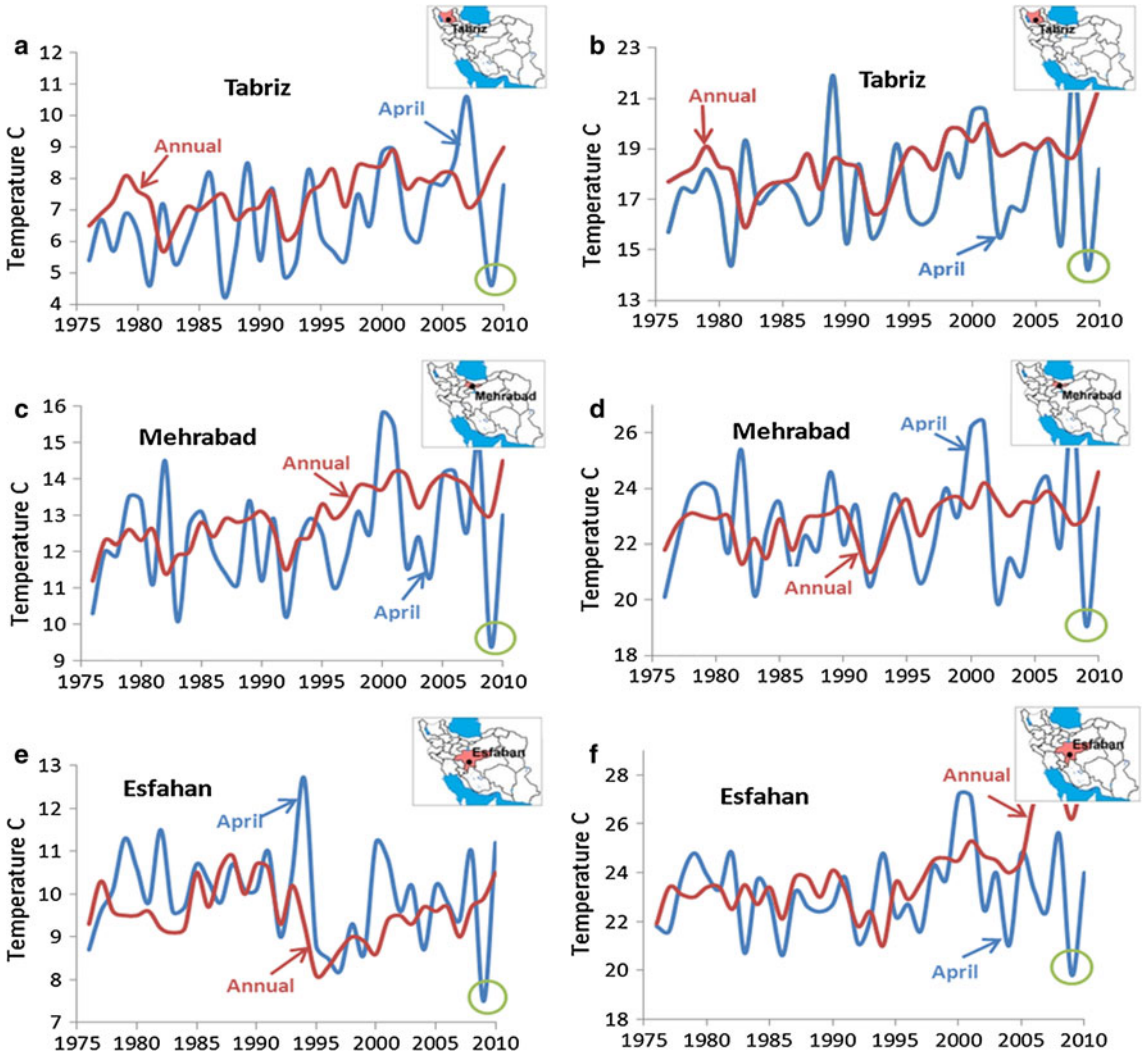

Fig. 6 The time series of line graphs for the minimum (**a**, **c**, **e**) and maximum (**b**, **d**, **f**) temperature (°C) for annual values and April values in the selected stations, viz Tabriz, Mehrabad (Tehran) and Esfahan stations. Each individual station is a representative of that geographical location in the country. The small map on the *top right corner* shows the location of the station in the country

varying between 1×10^{-5} s^{-1} and 5×10^{-5} s^{-1} (Fig. 3a). On the surface, the mean SLP indicates a ridge of large-scale anticyclone centered over the Black Sea extending southward and prevailing over the northern parts of Iran on April 12, 2009, resulting in a very cold advection from high latitudes over the northern half of the country. Simultaneously, a low center (1,014 hPa) located north of the latitude 50°N over Siberia area influenced the study area to some extent.

The circulation is characterized by a remarkable intensification of the pressure gradient due to the presence of a deep trough positioned over the Caspian Sea with its axis oriented along the northwest–southeast direction in the northern half of Iran (Fig. 7b). The meridional circulation pattern over the northwest parts of the country resulted in a very cold air influx from the Polar regions into Iran. The map of 1,000–500 hPa thickness (measured in m) indicates a relation with sea-level pressure contours with increasing values of isobars over the northern region of Iran, representing a high pressure and drop in temperature over the region. Besides, temperature values show warm air over the southeast areas of the country and cold air across the Zagros Mountain range due to the circulation pattern of the atmosphere.

Therefore, an intense pressure gradient developed as a result of thermal contrast between the borders of the two air masses (Fig. 7b). Figure 8 presents the vertical thermodynamic and dynamic structure for 0000 UTC of April 12, 2009 for the Tabriz radiosonde station. In the sounding diagram, ICE structural icing (light green) displays rime icing type. Rime ice is generally detected in conditionally unstable lapse rate environments. It is a rough, milky, opaque ice formed by the instantaneous freezing of small supercooled droplets as they strike the aircraft. The fact

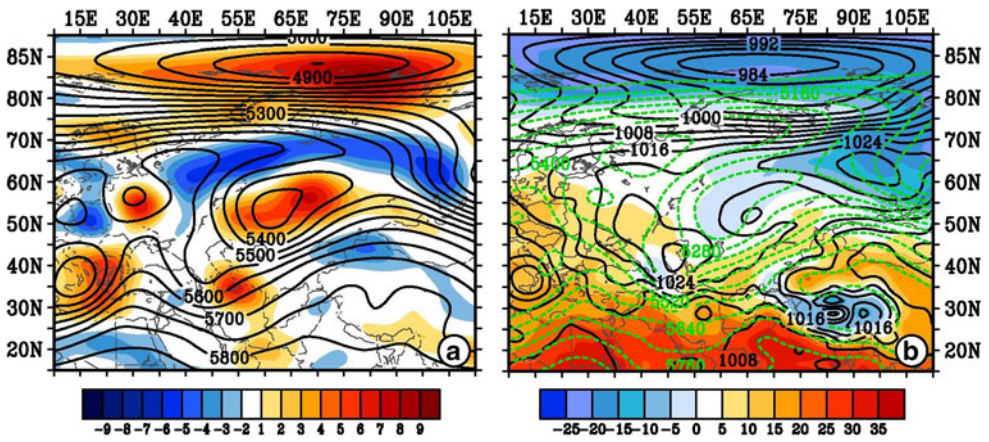

Fig. 7 **a** *Bold black contours* indicate mean geopotential height, and relative vorticity pattern is represented in *shaded* color contour at 500 hPa; **b** *solid dark contours* indicate mean sea-level pressure, *dashed green contours* indicate 1,000–500 hPa thickness and the *shaded background* is surface air temperature. The units for the parameters are: relative vorticity, 10^{-5} s^{-1}; geopotential height, m; sea-level pressure hPa and 1,000–500 thickness, m; surface air temperature, °C. The charts are valid on April 12, 2009

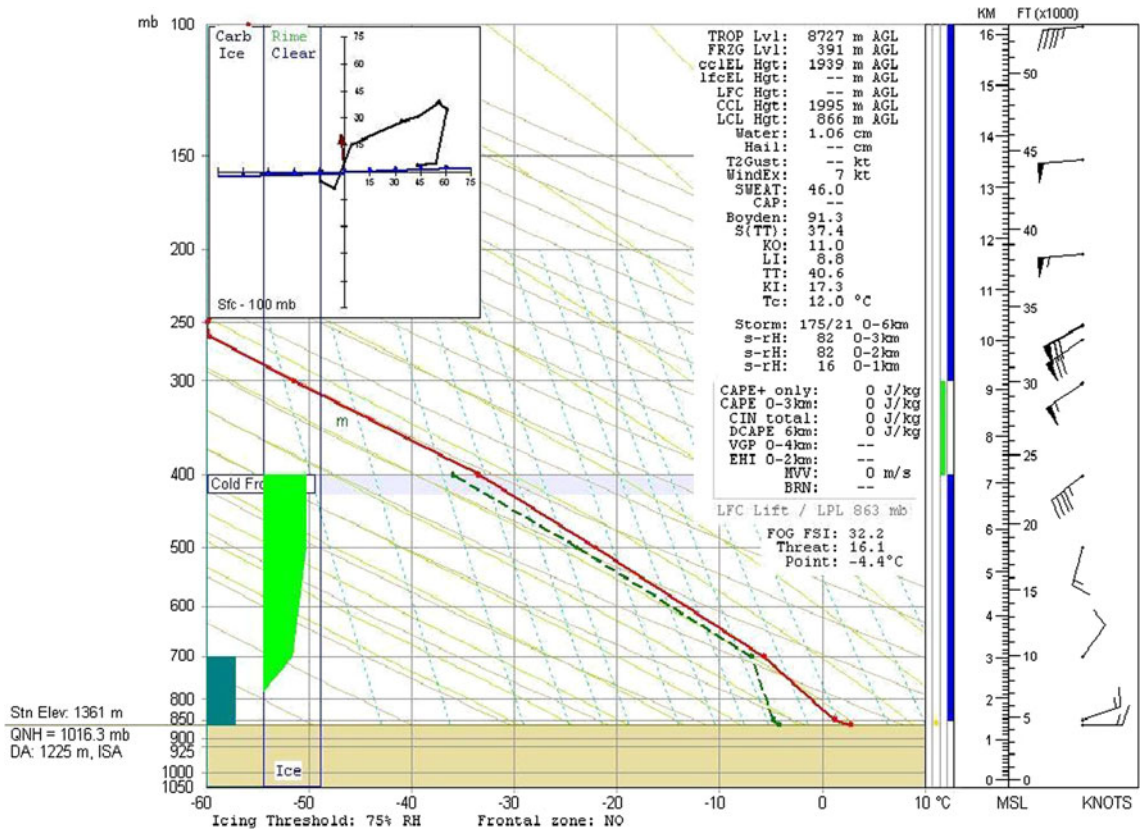

Fig. 8 Sounding vertical profile valid at 0000 UTC on April 12, 2009 for Tabriz radiosonde station (38°05′N, 46°17′E). The units for the parameters are: pressure, hPa; wind components, m s^{-1}; relative humidity, %; temperature, °C; CAPE value, J/kg

that droplets maintain their nearly spherical shape upon freezing and thus trap air between them gives rise to the formation of ice and its opaque appearance and makes it porous and brittle. The ICE structural icing occurred between 800 and 400 hPa levels.

Here, we used the *United States Air Force* (USAF) icing method to analyze the rime ice. In fact, USAF method is a function of *relative humidity* (RH) threshold values, i.e, 75 % and the presence of a frontal zone. The analyses indicate that the relative humidity properly distributed at

the multiple layers of the atmosphere; in particular at the lower levels, it varied between 65 and 91 %. Carburetor icing is indicated in the figure for the vertical thermodynamic structure (in dark green color). The carburetor (or induction) icing is most prevalent in warm and moist air. It is a function of ambient air temperature and dew point temperature, which occurred between 900 and 700 hPa levels at 0000 UTC April 12, 2009 in Tabriz radiosonde station (38°05′N, 46°17′E). It is recognized as moderate icing in the categories of icing severity. The speed and direction of the wind in the vertical structure indicate that the wind speed increases with elevation up to 9 km height (exceeds 36 m s^{-1}).

The storm motion and prevailing wind direction as represented in the vertical structure (upper left indicated in purple color) is northerly. The tropopause line is colored in purple at 263 hPa level in which the troposphere and stratosphere boundary is divided. A cold front can be detected in the vertical structure at 400 hPa. Due to the absolutely stable lapse rate prevailing in the lower atmosphere, the *convective available potential energy* (CAPE) value for the case is 0 J/kg (Fig. 8). Other thermodynamic parameters such as LCL, hail, energy and helicity indices, etc. are displayed in the upper right portion of the figure. In addition, other upper air variables for Tabriz radiosonde station in different levels of the atmosphere are shown for April 12, 2009 in Table 2.

The minimum temperature at 2 m height and wind flows at 10 m above the ground on April 12, 2009 are shown in Fig. 9a. The minimum temperature values were coincided well with the surface temperature values in Fig. 7b. The northern half of the country was influenced by the cold advection. Wind vectors, as the figure indicates, blow southward over the country exceeding 10 m s^{-1}. At 850 hPa level and relative humidity, streamlines fields of the u and v wind components are shown in Fig. 9b. The northeasterly winds blew over Iran and became westward due to the influence of the cyclonic system over the northern latitudes as well as a closed high-pressure center over the north of Afghanistan.

The moisture-rich wind from the Arabian Sea and Persian Gulf fed the moisture and then extended to the central and western parts of the country. Accordingly, cold air advection from high latitudes extended upon Iran by a high ridge centered over the north of the Black Sea and resulted in an intense pressure gradient and eventually a relatively strong cold front formed at 700 hPa (Fig. 10). In most parts of the country, the relative humidity values varied between

Table 2 Important upper air variables for Tabriz radiosonde station (38°05′N, 46°17′E) valid at 0000 UTC on April 12, 2009

Levels (hPa)	Temp (°C)	Mixing ratio (g/kg)	Dry bulb temp (°C)	Wet bulb temp (°C)	Dew point temp (°C)	Relative humidity (%)	Wind speed (m s^{-1})
Surface	2.8	5.3	6.7	5.6	−4.2	60	7.2
850 hPa	2	5.5	15.1	9.7	−7.1	60	7.5
700 hPa	−5.7	3.5	23.5	11.1	−6.9	91	5.7
500 hPa	−22.1	1.3	33.0	12.3	−23.9	85	8.2

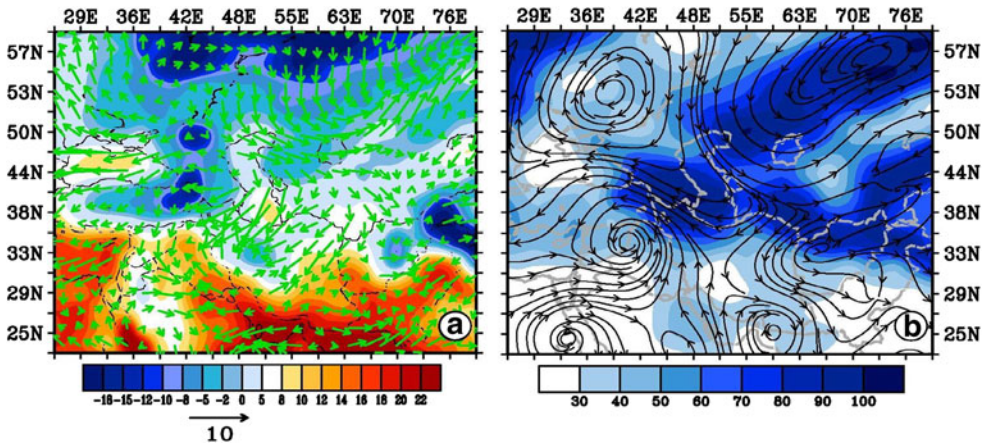

Fig. 9 **a** u and v wind components in green vectors, and minimum temperature at 2 m above the ground is represented in *shaded* color background; **b** mean relative humidity at 850 hPa height is represented as background of chart in *blue shade*, and streamlines are drawn in *black* barbs. The units for the parameters are: temperature, °C; relative humidity, %; wind flow, m s^{-1}. Figures are valid on April 12, 2009

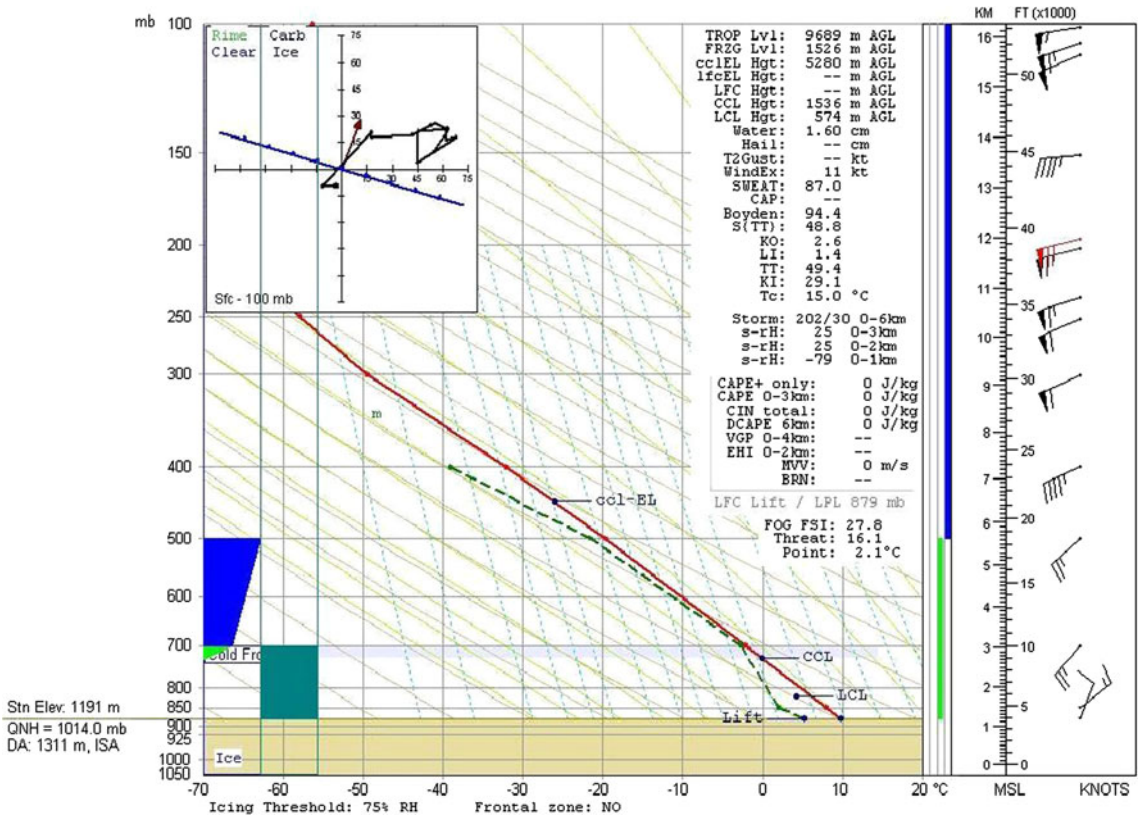

Fig. 10 Sounding vertical profile valid at 1200 UTC on April 13, 2009 for Tehran radiosonde station (35°41′N, 51°19′E). The units for the parameters are: pressure, hPa; wind, m s^{-1}; relative humidity, %; temperature, °C; CAPE value, J/kg

30–50 % apart from a small section over the northwest, in which it was more than 80 % causing snowfall in some stations in that area. Figure 10 presents the vertical profile at 1200 UTC of April 13, 2009 for Tehran radiosonde station. In the figure, ICE structural icing (dark blue) displays clear icing type. In fact, clear ice is detected in absolutely stable lapse rate environments. It is a glossy, clear or translucent ice formed by the relatively slow freezing of large supercooled droplets. The large droplets spread out over the airfoil of an airplane before complete freezing, forming a sheet of clear ice.

The ICE structural icing occurred at different levels of the atmosphere from 700 hPa through 500 hPa. Here, the USAF icing method is also used to analyze the clear ice. The analyses indicated that the relative humidity distributed at the lower levels of the atmosphere varied between 66 and 96 %. Another function shown in the vertical profile is carburetor icing (dark green). It occurred between 900 and 700 hPa levels and was recognized as a serious icing in the categories of increasing icing severity. The wind speed and direction indicated that the wind speed increased with height up to 11 km, exceeding 36.0 m s^{-1}. The storm motion and prevailing wind direction were observed as northeasterly. A cold front occurred at the level of 700 hPa and the CAPE value was 0 J/kg (Fig. 10). The tropopause line is colored in purple at the 237 hPa level. In this vertical profile also some other main upper air level variables for Tehran radiosonde station (35°41′N, 51°19′E) at multiple levels of the atmosphere on April 13, 2009 are shown in Table 3.

The horizontal divergence and convergence fields and the wind on April 12, 2009 are shown in Fig. 11a. According to the figures, the convective fields (blue shading) were clearly observed over the northern half of Iran varying between 2×10^{-6} s^{-1} and -12×10^{-6} s^{-1}. The northerly winds simultaneously at 1,000 hPa level that blew toward the negative fields (convective areas) over the region exceeded 10 m s^{-1}. Accordingly, the cross section of the horizontal divergence and convergence fields and wind at latitude 37°N coincided well with the 1,000 hPa level, so that the convergence fields at the surface level were replaced with those of the divergence fields at the upper levels. The wind pattern at the upper level was westerly, as well (Fig. 11b).

Figure 11 clearly shows a northerly wind flow from the surface to the upper levels of the atmosphere over the region under study. Finally, to visualize the synoptic conditions, meteorological satellite pictures are provided for

Table 3 Important upper air level variables for Tehran radiosonde station (35°41′N, 51°19′E) valid at 1200 UTC on April 13, 2009

Levels (hPa)	Temp (°C)	Mix ratio (g/kg)	Dry bulb temp (°C)	Wet bulb temp (°C)	Dew-point temp (°C)	Relative humidity (%)	Wind speed (m s^{-1})
Surface	9.8	8.6	17.7	14.0	5.2	73	5.1
850 hPa	8	8.7	22.9	16.0	2	66	7.7
700 hPa	−2.1	4.8	27.0	13.8	−2.7	96	13.9
500 hPa	−19.7	1.6	35.7	13.6	−21.5	86	12.9

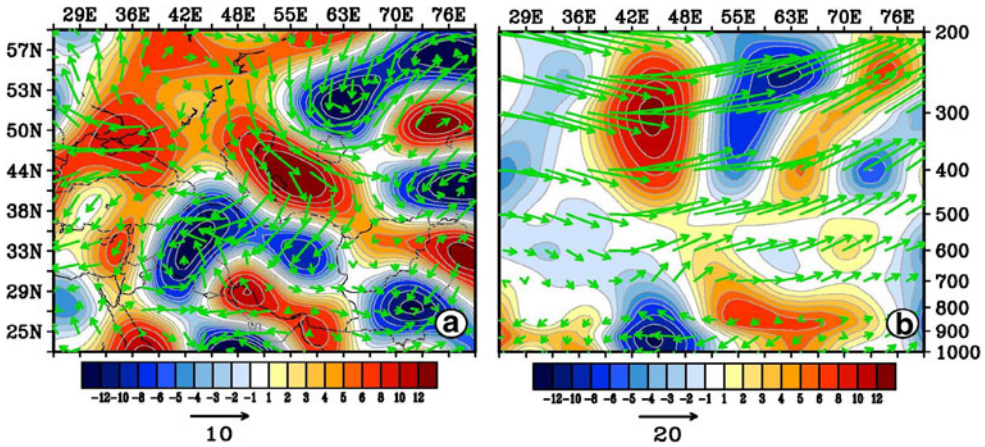

Fig. 11 **a** Mean horizontal divergence and convergence fields and wind at 1,000 hPa; **b** mean vertical cross section for horizontal divergence and convergence fields and wind at latitude 37°N. The units for the parameters are: divergence and convergence fields, 10^{-6} s^{-1}; wind flow, m s^{-1}. The figures are valid on April 12, 2009

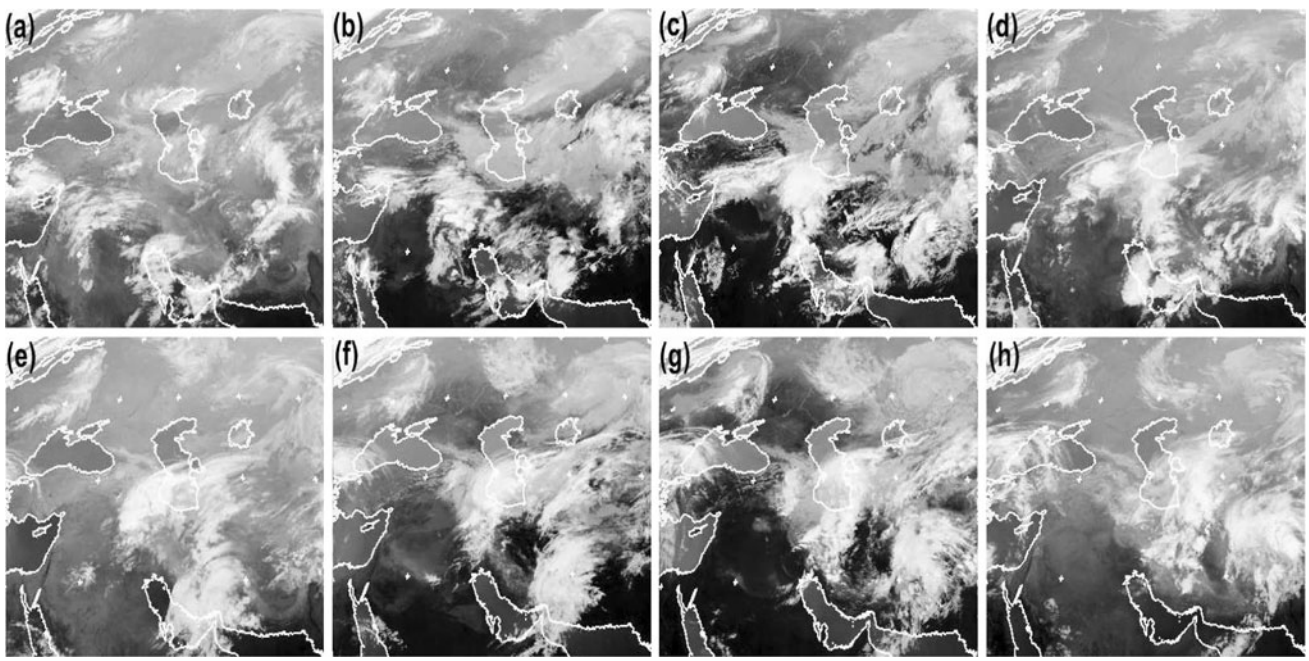

Fig. 12 Metosat VISSR (IODC) images valid at **a** 0000 UTC, **b** 0600 UTC, **c** 1200 UTC, **d** 1800 UTC on April 12, 2009; **e** 0000 UTC, **f** 0600 UTC, **g** 1200 UTC and **h** 1800 UTC on April 13, 2009. (http://www.sat.dundee.ac.uk)

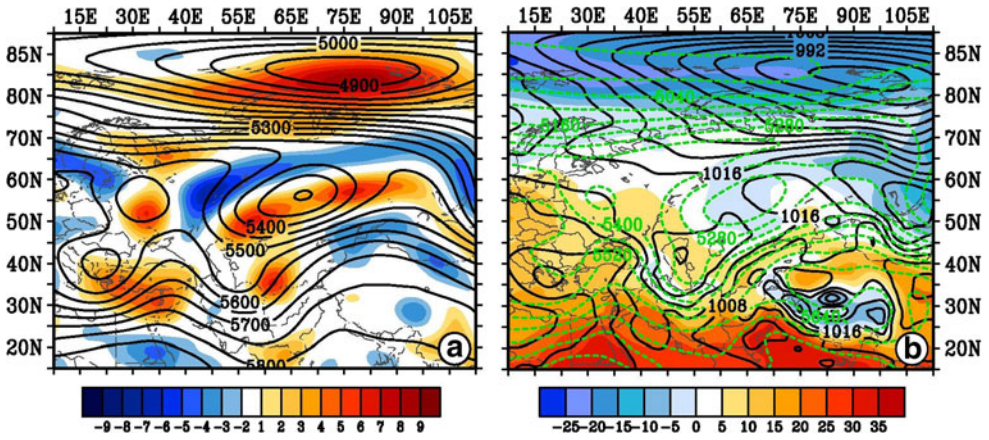

Fig. 13 **a** *Bold black contours* indicate mean geopotential height, and relative vorticity at 500 hPa is presented as *shaded* in the background; **b** *solid dark contours* indicate mean sea-level pressure, *dashed green contours* indicate 1,000–500 thickness and the *shaded* background is surface air temperature. The units for the parameters are: relative vorticity, 10^{-5} s^{-1}; geopotential height and 1,000–500 thickness, m; sea-level pressure, hPa; surface air temperature, °C. The figures are valid on April 14, 2009

the frost event under study. In the early hours of the event, i.e., 0000 UTC on April 12, 2009, as the satellite images indicate, the onset of clouds over the western parts of Iran was clearly observed (Fig. 12a–d) and within the next day, i.e., on April 13, 2009, the cloud systems gradually moved eastward and covered the whole country (Fig. 12e–h) causing snowfall and reduction in temperature below zero in most parts of the country, especially over the mountainous regions (Fig. 2a, b). Therefore, since the sky is absolutely clear and there are no clouds when a radiation frost occurs, the cloudiness clearly confirmed the occurrence of an advective frost over the region. Hence, we can infer that there is a link and association between cloudiness and advective frost.

4.1.2 Weather charts analysis on April 14, 2009

The map of 500 hPa relative vorticity and geopotential height for April 14, 2009 is shown in Fig. 13a. As the contours indicate, the polar vortex extends toward the lower latitudes. The closed low center with geopotential height of 5,325 hPa moved eastward, located at longitude 70°E, and its ridge completely covered the entire Iran. On this day, i.e., April 14, 2009, positive vorticity was evident, coinciding with the low center in the geopotential height field varying between 1×10^{-5} s^{-1} and 6×10^{-5} s^{-1} (Fig. 13a). A cutoff low was generated within the cold system center as a result of the meridional circulation possessing a huge thermal difference as compared to the adjacent air (Fig. 13b). The average temperature decreased to less than −5 °C in the low center. The system cells displaced toward southeast and provided a suitable pressure gradient over the northern border of Iran on April 13, 2009 (not shown). In the long run, the cold system prevailed over the entire study area excluding the southern border of the country, resulting in a vernal late advective cooling event in most regions of the land; the intense isobars of 1,000–500 thickness and its deep trough over the country confirmed such a condition.

The cold system on the next day left the study area toward east. As a result, the temperature over the eastern and southern parts of the country began to increase on April 15 (not shown). Figure 14 presents the vertical profile at 1200 UTC of April 14, 2009 for Tehran radiosonde station (35°41′N, 51°19′E). In the sounding diagram, ICE structural icing (dark blue) displays clear icing type. It occurred at the 700 hPa level to some extent. Here, the USAF icing method is also used to analyze the clear ice. The relative humidity distributed at the lower levels of the atmosphere varied between 56 and 80 %. Carburetor icing (dark green) occurred between 900 and 700 hPa levels and recognized as moderate icing in the categories of increasing icing severity. The vertical profiles of wind speed and direction indicated that the wind speed intensified with elevation up to 7.5 km height, exceeding 48.9 m s^{-1}.

The storm motion and prevailing wind direction were observed to be southeasterly. The vertical profile of temperature brought out the tropopause at 197 hPa (line colored in purple) and a cold front was detected at 400 hPa. The CAPE value corresponding to the vertical profile at 1200 UTC of April 14, 2009 for Tehran was 179 J/kg due to a relatively unstable environment at the lower level (Fig. 14). Other upper air variables for Tehran radiosonde station at different levels of the atmosphere on April 14, 2009 are shown in Table 4.

The minimum temperature at 2 m height and wind flows at 10 m above the ground on April 14, 2009 are shown in Fig. 15a. The minimum temperature values varied between

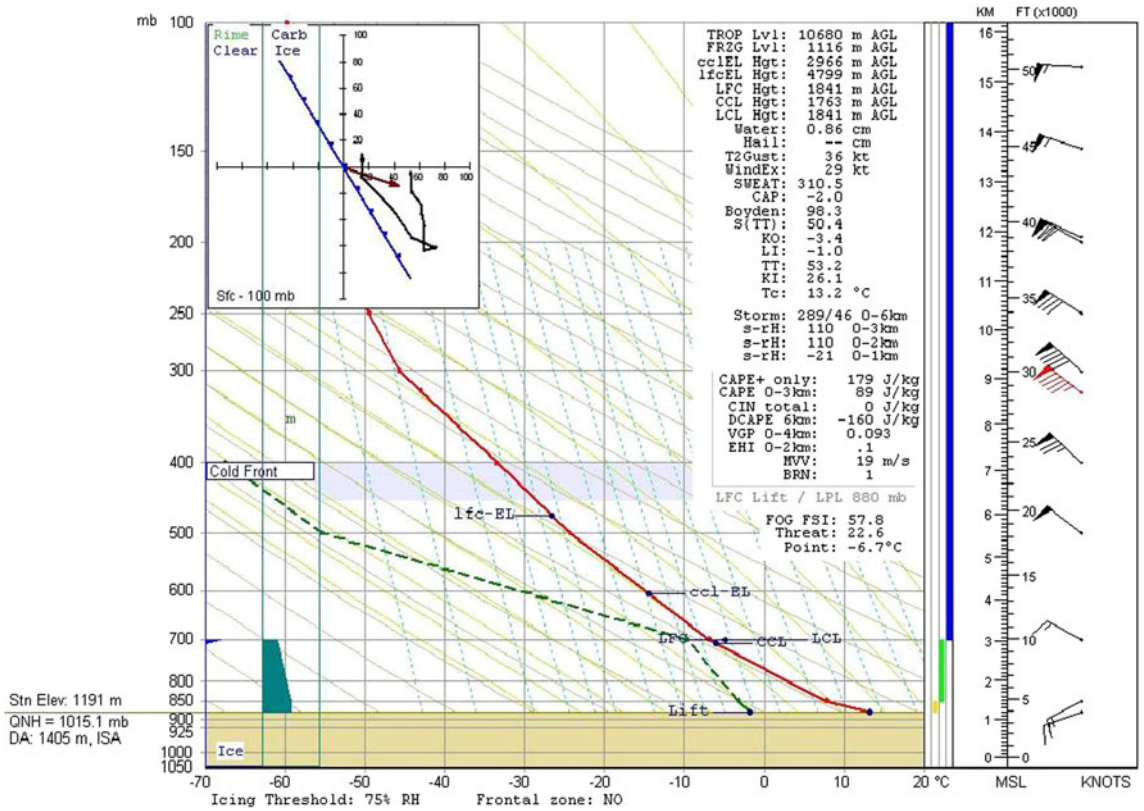

Fig. 14 Sounding vertical profile valid at 1200 UTC on April 14, 2009 for Tehran radiosonde station (35°41′N, 51°19′E). The units for the parameters are: pressure, hPa; wind components, m s^{-1}; relative humidity, %; temperature, °C; CAPE value, J/kg

Table 4 Important upper air variables for Tehran radiosonde station (35°41′N, 51°19′E) valid at 1200 UTC on April 14, 2009

Levels (hPa)	Temp (°C)	Mix ratio (g/kg)	Dry bulb temp (°C)	Wet bulb temp (°C)	Dew-point temp (°C)	Relative humidity (%)	Wind speed (m s^{-1})
Surface	13.2	10.0	16.5	14.8	−1.8	35	8.2
850 hPa	7.8	9.0	24	16.6	−3.2	46	8.8
700 hPa	−6.9	3.6	23.2	11.0	−9.7	80	8.2
500 hPa	−24.3	1.1	30.5	11.0	−55.3	4	25.7

4 and −6 °C over the study area. Most parts of the country were influenced by cold advection. Wind vectors, as the figure indicates, intensified exceeding 10 m s^{-1} over the country (Fig. 15a). Besides, at the isobaric level of 850 hPa (Fig. 15b), most parts of the country surrounded by northerly flows due to an anticyclonic activity over latitude 50°N and longitude 24°E caused cold air advection from high latitudes into Iran, as most stations under study experienced a temperature below 0 °C.

The humidity feeding ceased in all regions of Iran as well. As a result of a large-scale cyclonic activity over Turkey, on the next day, the circulation direction changed and warm air advection occurred from the lower latitudes on April 15, 2009 over the eastern and southern parts of the country (not shown). Figure 16 presents the vertical profile of temperature and humidity at 1200 UTC April 15, 2009 for Mashhad radiosonde station (36°16′N, 59°38′E). In the sounding diagram, ICE structural icing (light green) displays rime icing type. It occurred at 700 hPa level to some extent. The relative humidity distributed at the lower levels of the atmosphere varied between 66 and 91 %.

Carburetor icing occurred between 900 and 700 hPa levels and was recognized as serious in the categories of increasing icing severity. The vertical profile of wind speed and direction indicated that the wind intensified with elevation up to 9.5 km height exceeding 43.9 m s^{-1}. The storm motion and prevailing wind direction were observed to be northeasterly. The tropopause line colored in purple was measured at 216 hPa level. In this sounding diagram, a cold front was also detected at 700 hPa and the CAPE

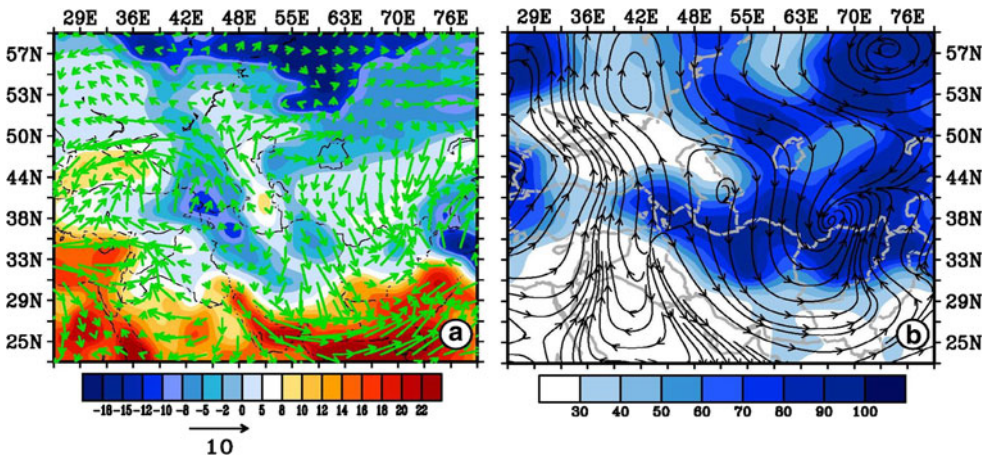

Fig. 15 **a** u and v wind components (m s^{-1}) in green vectors, and minimum temperature (°C) at 2 m above the ground is shown shaded in color as background of chart; **b** mean relative humidity (%) at 850 hPa height is represented in *blue shaded* background and streamlines are drawn in *black* barbs. The units for the parameters are: temperature, C; relative humidity, %; wind flow, m s^{-1}. Figures are valid on April 14, 2009

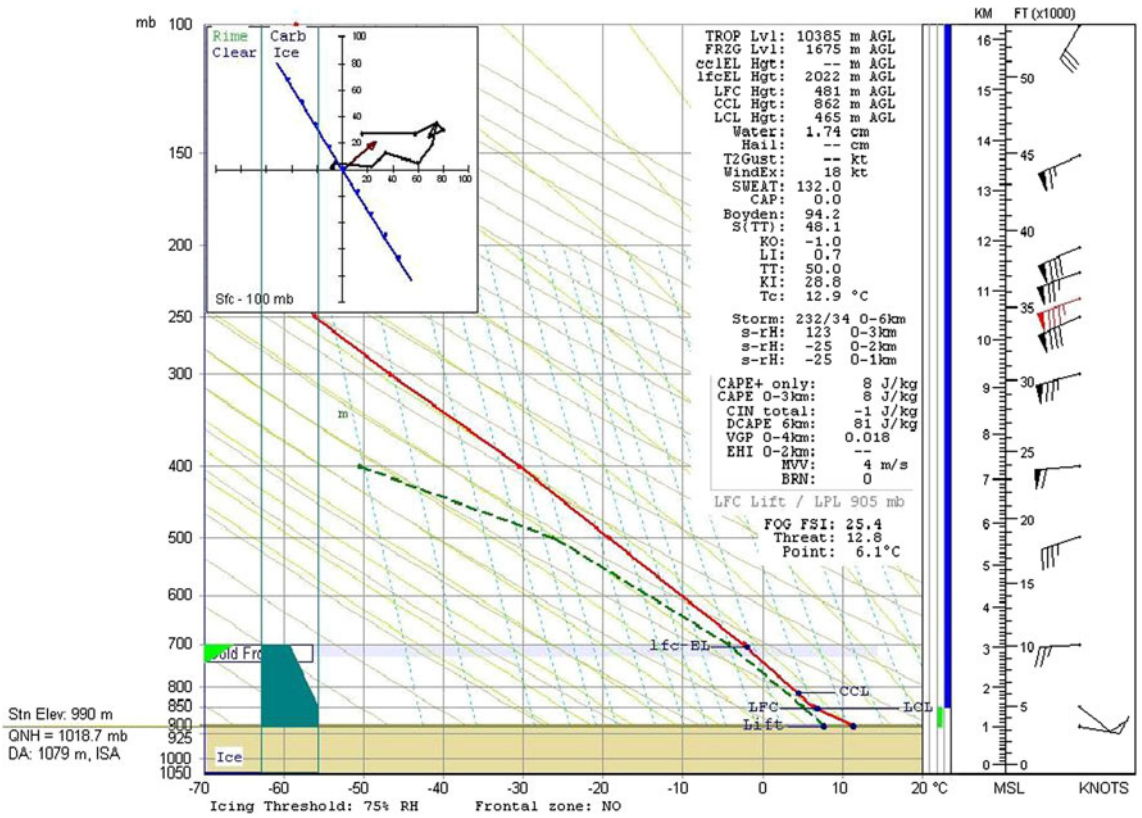

Fig. 16 Sounding vertical profile valid at 1200 UTC on April 15, 2009 for Mashhad radiosonde station (36°16′N, 59°38′E). The units for the parameters are: pressure, hPa; wind components, m s^{-1}; relative humidity, %; temperature, °C; CAPE value, J/kg

value was 8 J/kg (Fig. 16). Other upper air variables for Mashhad radiosonde station at different levels of the atmosphere on April 15, 2009 are shown in Table 5.

The horizontal divergence fields and wind on April 14, 2009 are shown in Fig. 17a. According to the figures, the divergence fields extended over most parts of Iran varying between -2×10^{-6} s^{-1} and -12×10^{-6} s^{-1}. Simultaneously, winds exceeding 10 m s^{-1} at 1,000 hPa blew toward south in the region of negative divergence fields over the region. Accordingly, the cross section of the horizontal divergence fields and the wind at latitude 37°N coincided well with the 1,000 hPa level, in such a way that the convergence fields at the surface level were replaced by those of the divergence fields at the upper levels, and the wind patterns at the upper levels were westerly (Fig. 17b).

On the whole, maps in Fig. 17 clearly showed a northerly wind flow over the region. On the third day of the event, i.e., 0000 UTC on April 14, 2009, as the satellite

Table 5 Important upper air level variables for Mashhad radiosonde station (36°16′N, 59°38′E) valid at 1200 UTC on April 15, 2009

Levels (hPa)	Temp (°C)	Mix ratio (g/kg)	Dry bulb temp (°C)	Wet bulb temp (°C)	Dew-point temp (°C)	Relative humidity (%)	Wind speed (m s^{-1})
Surface	11.2	8.2	13.6	12.0	7.7	78	4.1
850 hPa	6.4	7.5	21.3	14.3	5.0	91	4.1
700 hPa	−2.3	4.6	26.9	13.5	−4.2	87	11.8
500 hPa	−19.3	1.7	36.7	14.1	−26.3	54	18.5

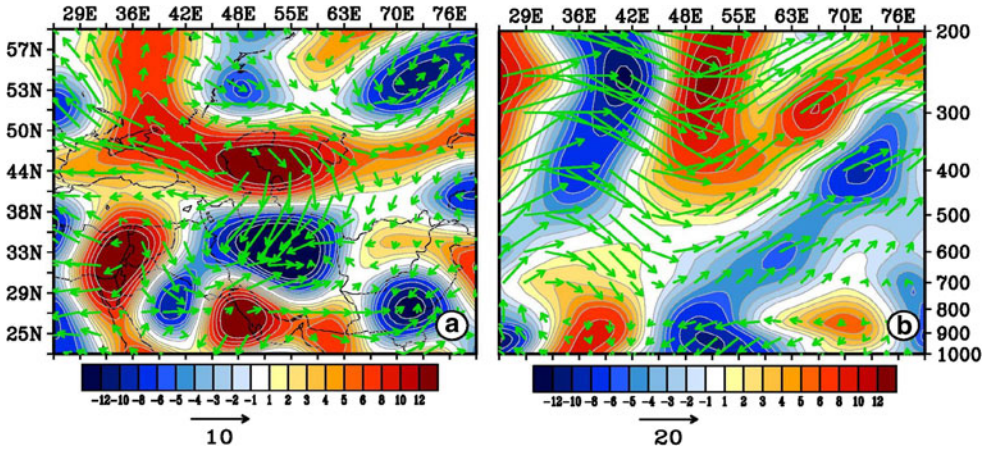

Fig. 17 **a** Mean horizontal divergence and convergence fields and wind at 1,000 hPa; **b** mean cross section for horizontal divergence and convergence fields and wind at latitude 37°N. The units for the parameters are: divergence and convergence fields, 10^{-6} s^{-1}; wind flow, m s^{-1}. The figures are valid on April 14, 2009

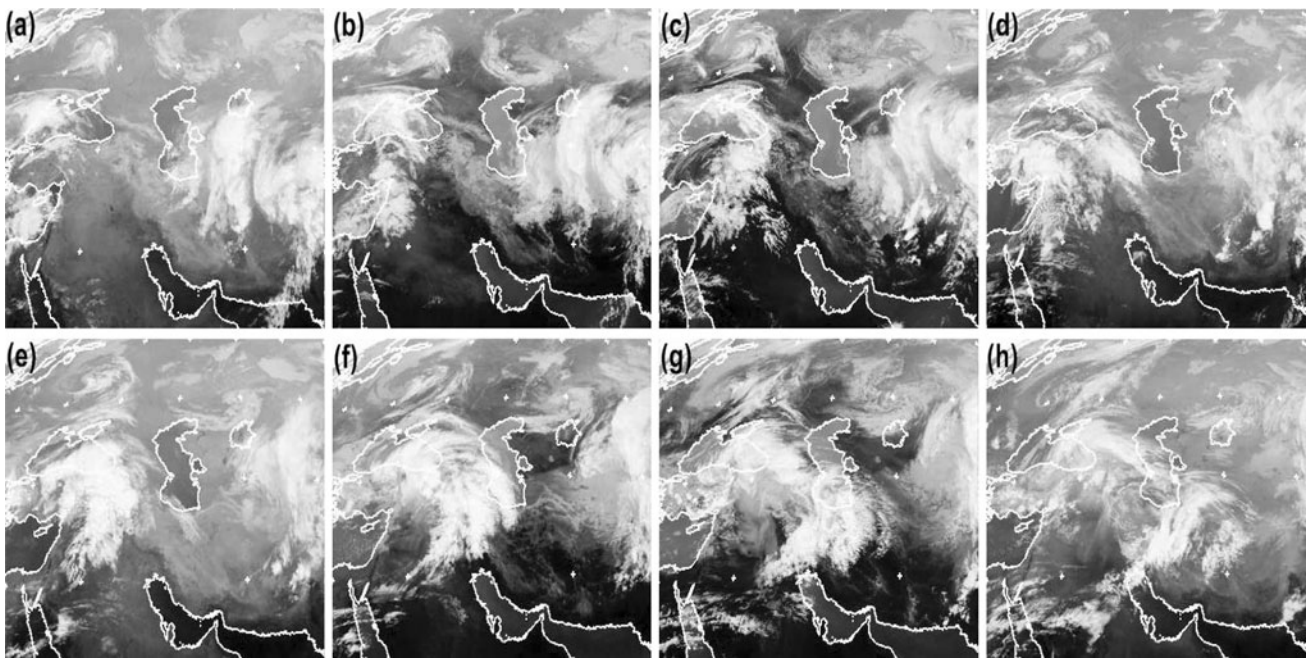

Fig. 18 Metosat VISSR (IODC) images valid at **a** 0000 UTC, **b** 0600 UTC, **c** 1200 UTC, **d** 1800 UTC on April 14, 2009; **e** 0000 UTC, **f** 0600 UTC, **g** 1200 UTC and **h** 1800 UTC on April 15, 2009

images indicate, the cloud system moved to the northeast parts of the country (Fig. 18a–d) and within the next day, i.e., on April 15, 2009, the cloud systems re-covered most part of the country (Fig. 18e–h) causing snowfall and reduction in temperature below zero in the northern half of the country (Fig. 2c, d).

4.2 HYSPLIT trajectory model and temperature advections

A backward trajectory Lagrangian model was applied to investigate further the weather conditions throughout the period of the cooling event. The model was run for the event in two stations, viz Tabriz (38°05′N, 46°17′E) and Tehran (35°41′N, 51°19′E) stations, ending at the peak time and ending time of the cooling event valid at 0600 UTC of 14 April and 2300 UTC of 15 April 2009, each one with 48 h run duration. The backward trajectories' cross sections are shown at the bottom of Fig. 19a, b. It demonstrates the different levels above ground, viz 500, 1,500 and 5,000 m AGL in three different colors, i.e., red, blue and green, respectively. The result indicates that at the peak time of the cooling event, the air parcels in the selected stations at lower levels, i.e., 500 and 1,500 m above ground levels, originating mostly from the Caspian Sea and the western surrounding areas (Fig. 19a) due to the influence of the anticyclone over the region (Fig. 13b).

At the same time, a large-scale cyclonic circulation originating from the polar vortex was responsible for the cooling event over the country at the middle and upper levels, viz 5,000 m AGL. At this level, the air parcels came from far away areas mainly over the Polar region to the study area through northerly winds (v-component) owing to the extraordinary development of the polar vortex resulting in an intense and abnormal cooling event over Iran (Fig. 19a). The backward trajectories with ending at

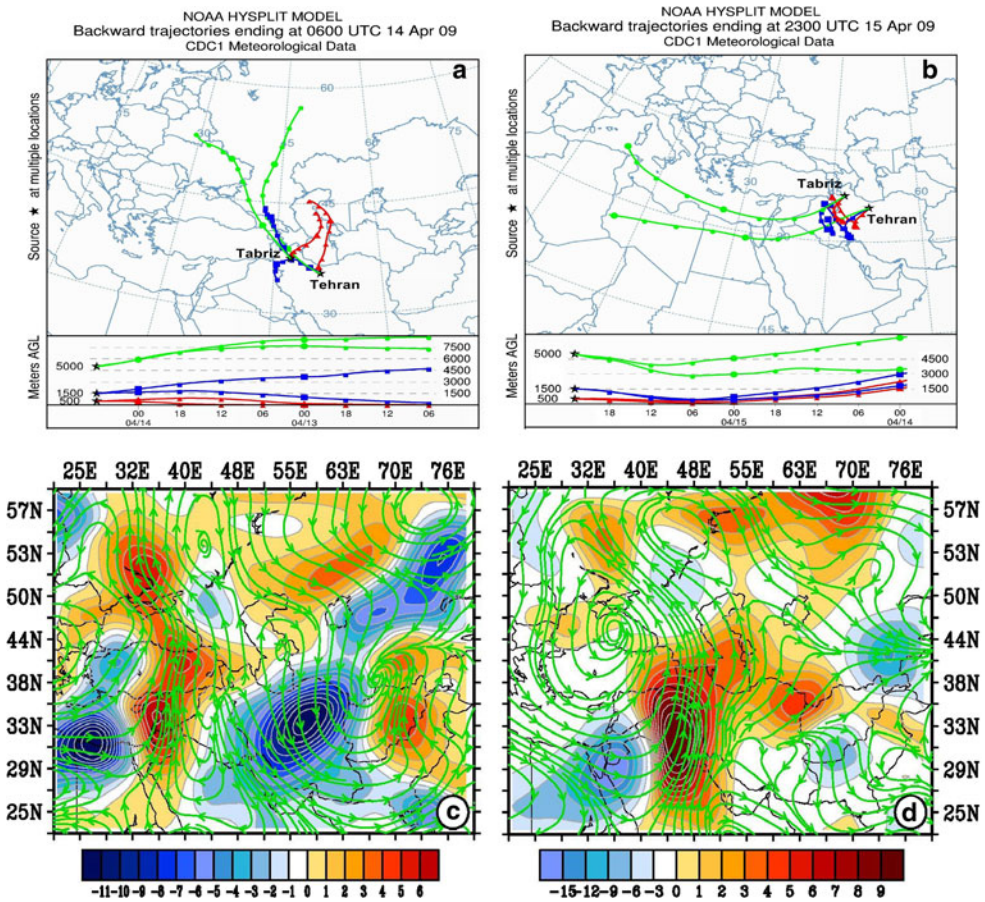

Fig. 19 HYSPLIT model backward trajectory outputs ending at the peak time (**a**) and ending time (**b**) of the cooling event valid at 0600 UTC of 14 April 2009 and 2300 UTC of 15 April 2009, respectively. The model ran for 48 h and used 6 h time steps (nodes). The figure demonstrates the individual air parcels at three levels [500, 1,500 and 5,000 m above ground level (AGL)] selected at Tabriz (38°05′N, 46°17′E) and Tehran (35°41′N, 51°19′E) stations. Backward trajectory cross sections were included in the bottom of each figure for the same level. Cold and warm air temperature advections with wind streams overlaid (**c**, **d**) were produced for 850 hPa level on April 13 and April 15, 2009, respectively. Air advections charts were produced using three meteorological variables including 850 hPa u and v wind components and air temperature variables. Air temperature advection is in terms of Kelvin per day (K/day)

end time on 2300 UTC of 15 April 2009 in Tabriz and Tehran stations (Fig. 19b) also indicate the end of the cooling event over the region as a result of arrival of the hot air parcels from Iraq—in lower levels (500 and 1,500 m AGL), and also from far away regions viz north of Africa—in upper levels (5,000 m AGL). The HYSPLIT model outputs confirm the synoptic analyses for the cooling event discussed above.

Additionally, we tried to display cold and warm air temperature advections at 850 hPa level for the cooling event (Fig. 19c, d). In fact, temperature advection is that portion of the local temperature tendency due to the wind blowing across the isotherms. The cold air advection is shown in Fig. 19c. It clearly shows the advection of freezing air temperature values varying between 0 and -11 Kelvin/day over Iran in the central part of the country on April 13, 2009 (Fig. 19c), while the warm air advection, which is presented in Fig. 19d, obviously illustrates the advection of hot air values varying between 1 and 9 K/day over the western areas showing the end of the cooling event over those regions on April 15, 2009 (Fig. 19d). It is worthwhile to mention that for the air advection charts produced using three variables, to verify the outputs, we overlaid the wind streams and found that, as Fig. 19c, d indicate, there is good agreement between the air temperature advections and the direction of winds (Fig. 19c, d).

5 Conclusions

During April 12 through 15, 2009 a severe cold system occurred over almost entire Iran resulting in a considerable drop in temperature that caused snowfall over most parts of the country. This is identified as a most intense advective cooling event that occurred within a couple of recent years. The meteorological aspects of the formation of the intense cooling system were studied based on synoptic and thermodynamic structure of the atmosphere and we bring out the following findings:

1. The 500 hPa contours indicated that the polar vortex was responsible for the frost event over the country extending largely southward and its ridge influenced most parts of Iran. This was recognized as an unusual extension of the polar vortex in the recent years. The relative vorticity values at the center of 500 hPa geopotential height field during the study period varied between 1×10^{-5} s^{-1} and 6×10^{-5} s^{-1}.
2. On the surface chart, the mean SLP indicated a ridge of large-scale anticyclone centered over Black Sea extending southward, prevailing over most parts of Iran and resulting in a severe cold air advection from high latitude over Iran. The meridional circulation pattern over the country resulted in a severe cold air influx from the Polar regions into Iran. The minimum temperature values at 2 m above the ground were coincident with those of surface temperature values. The wind vector at 10 m height was directed southward over the country exceeding 10 m s^{-1}.
3. During the study period, the prevailing wind at 850 hPa was southward in most parts of the country due to the presence of the anticyclone centered over latitude 50°N and longitude 24°E, resulting in a cold air advection from high latitudes to Iran. This caused a reduction in temperature below 0 °C. In addition, moisture was fed to the study area by the Arabian Sea and Persian Gulf during the period. In most parts of the country, the relative humidity values were between 40 and 90 % apart from the southern coasts of the country.
4. Convergence fields were observed over Iran (between -2×10^{-6} s^{-1} and -12×10^{-6} s^{-1}) during the study period. Simultaneously, the southward wind at 1,000 hPa level blew toward the region of convergence. The wind cross section indicated a high level of harmony with the divergence and convergence wind fields.
5. The vertical profiles of temperature and humidity indicate that the ICE structural icing displayed both rime and clear icing types. As explained earlier, rime ice was detected in a conditionally unstable environment. On the contrary, clear ice was detected in an absolutely stable environment. The ICE structural icing occurred at multiple levels of the atmosphere, i.e., from 800 through 400 hPa levels. The analyses also brought out that the relative humidity distributed at multiple layers of the atmosphere, especially at the lower levels, varied between 65 and 96 %. Carburetor (or induction) icing, as a function of ambient air temperature and dew point temperature, occurred between 900 and 700 hPa levels in the selected radiosonde stations during the study period. Besides, the vertical profiles of wind speed and direction indicated that the wind intensified between 7.5 and 9.5 km with a speed between 36.0 and 48.9 m s^{-1}. In the vertical profile, symptoms of cold fronts were observed between 700 and 400 hPa levels. Since the atmosphere was absolutely stable over most of the stations, the convective available potential energy (CAPE) values were zero or very small as reflected in the thermodynamic structure of the atmosphere for most of the radiosonde stations.
6. The backward trajectories also indicated that the cold air advection originated from higher latitudes as a result of an extraordinary extension of the polar vortex toward the lower latitude including Iran, resulting in an

abnormal cooling event over the country. The activity of the cooling event ended on arrival of hot air parcels (warm air advection) from Iraq (lower levels) and even north of Africa (upper levels). In general, the HYSPLIT model outputs were in quite good agreement with those of the synoptic features.

7. Finally, to visualize the synoptic conditions, meteorological satellite pictures for the frost event were employed during the study period. The presence of clouds clearly confirmed the occurrence of an advective cooling event over the region. Analysis of minimum temperature pattern during the study period confirms the arrival, development and leaving of the cold system over the country.

Acknowledgments The authors gratefully acknowledge the support extended by the organizations: for the availability of 24 h minimum temperature data provided by I.R. of Iran Meteorological Organization (IRIMO), the radiosonde data from the University of Wyoming, USA, and the infrared cloud imageries from the Dundee satellite receiving station, UK. We also gratefully appreciate the NOAA Air Resources Laboratory (ARL) for the provision of the HYSPLIT model and READY Web site used in this publication.

References

Nohi K et al (2007) Investigation of beginning and end of radiation—advective frosts date in northwest Iran. Natl J Res Cultiv Agri, Ministry of Agriculture, Tehran, no. 75 (in Persian)

Azizi GH et al (2009) Synoptic analysis of intensive cold surge of January 2007. Q Magazine Res Phys Geogr, Faculty of Geography, University of Tehran, Tehran, Iran, no. 70, pp 1–20 (in Persian)

Alijani B, Hajbarpour GH (2007) Synoptic analysis of frost in Ardabil province, geography and development magazine. Zahedan University, Iran (in Persian)

Alijani B (1996) Climate of Iran, Payam-e-Nour University press, Tehran, Iran (in Persian)

Azizi, GH. (2004) Synoptically assessment of extensive springtime frosts in western half of Iran. Quarterly Journal of Teacher Training University, Tehran, Iran, no. 81, pp 99–115 (in Persian)

Baraty GH (1999) Migration systematic relationships and Iranian vernal frosts. Q J Res Geogr, Isfahan, no. 53 (in Persian)

Bosart LF, Nocera JJ, Knight DJ (2000) Numerical simulation studies of South American cold air damming: a physical interpretation and assessment. 6th International conference on southern hemisphere meteorology and oceanography, Santiago. Chile, Santiago, pp 362–363

Dotty B (1996) The grid analysis and display system (GRADS), V1.5.1.12. http://www.iges.org/grads/gadoc/users.html

Draxler RR, Rolph GD (2011) HYSPLIT (HYbrid Single-Particle Lagrangian Integrated Trajectory) Model access via NOAA ARL READY Website. (http://ready.arl.noaa.gov/HYSPLIT.php)

Fattahi E, Salehipak T (2009) Analysis of the wintertime frosts synoptic patterns over Iran. J Geogr Dev 13:127–136 (in Persian)

Fortune MA, Kousky VE (1983) Two severe freezes in Brazil: precursors and synoptic evolution. Mon Weather Rev 111(181):196

Garreaud RD (1999) Cold air incursions over subtropical and tropical South America: a numerical case study. Mon Weather Rev 122:2823–2853

Garreaud RD (2000) Cold Air incursions over subtropical South America: mean structure and dynamics. Mon Weather Rev 128:2544–2559

Goodal GE, Angus DE, Leonard AS, Brooks EA (1957) Effectiveness of wind machine. Calif Agric 2:7–9

Hamilton G, Tarifa R (1978) Synoptic aspects of a polar outbreak leading to frost in tropical Brazil, July 1972. Mon Weather Rev 106:1545–1556

Kalnay E et al (1996) The NCEP/NCAR 40-year reanalysis project. Bull Am Meteorol Soc 77:437–471

Krishnamurti TN, Tewari M, Chakraborty DR, Marengo JA, Silva Dias PL, Satyamurti P (1999) Downstream amplification: a possible precursor to major freeze events over south-eastern Brazil. Weather Forecast 14:242–270

Marengo JA, Nobre C, Culf A (1997a) Climate impacts of the 'Friagens' in forested and deforested regions in Amazon Basin. J Appl Meteorol 36:1553–1566

Marengo JA, Cornejo A, Satyamurty P, Nobre C, Sea W (1997b) Cold surges in tropical and extratropical South America: the strong event in June 1994. Mon Weather Rev 125:2759–2786

Masoudian SA, Darand M (2012) Analysis of sea level pressure anomalies during extreme cold temperature days of Iran. Geogr Environ Plann J 45(1) (in Persian)

Omidvar K, Ebrahimi A (2012) The analysis of cold wave severity between 6 to 15 January 2008 in central provinces of Iran (Isfahan, Kerman and Yazd provinces). Geogr Environ Plann J 45(1) (in Persian)

Rahimi M (1999) An investigation of the occurrence probability of vernal late frosts and autumn early in central Alborz, MS Thesis, Faculty of Geography, University of Tehran, Tehran (in Persian)

Rolph GD (2011) Real-time Environmental Applications and Display sYstem (READY) website (http://ready.arl.noaa.gov). NOAA Air Resources Laboratory, Silver Spring

Snyder RL, Paulo J (2005) Frost protection: fundamentals, practice and economics, vol 1. Food and Agriculture Organization of the United Nations, Rome

Soltani M, Azizi GH, Hanafi A (2008) Using statistical models to frost analysis and prediction, a case study: Kurdistan Province of Iran. Q J Geogr LAUCTB, Literature and Humanity Faculty, vol 2, no. 5, Tehran (in Persian)

Stunder BJB (1997) NCEP Model Output—FNL ARCHIVE DATA, TD-6141. Prepared for National Climatic Data Center (NCDC). This document and archive grid domain maps are also available at http://www.arl.noaa.gov/ss/transport/archives.html

Vera CS, Vigliarolo PK (2000) A diagnostic study of cold-air outbreaks over South America. Mon Weather Rev 128:3–24